Ultrasonic Imaging Through Highly Reverberant Thin Layers— Theoretical Considerations

by J. Saniie, E. S. Furgason, and V. L. Newhouse

Abstract

Nondestructive testing of targets consisting of a finite number of thin layers is a particularly challenging problem in material evaluation. In principle, such objects can be evaluated by examining the backscattered echoes produced by an ultrasonic pulse-echo system and extracting those acoustical parameters sensitive to the inhomogeneity of the sample. In practice, extracting these parameters is difficult if not impossible because: 1) spatial resolution of the system is limited, and 2) multiple reflections within the target confound the measurements. In this study, the complex pattern of echoes is unraveled through the use of a simple classification scheme. An effective simulation algorithm, based on this classification, is presented and verified by experimental measurements. It is shown that after signal-to-noise ratio enhancement, a single class of echoes can be isolated from the backscattered signal. These techniques are then adapted for the particular reverberant structure faced in measuring support plate corrosion growth around steam generator tubes from inside the tube.

SI CONVERSION FACTOR
1 mil = 25.4 μm

INTRODUCTION

In most applications of ultrasonic imaging, reverberations do not play an important role, or at least are assumed to be insignificant. The principal exception in medical imaging arises when the interrogation must be made through bone. In this case, the multiple reflections produced by reverberations in the bone become the dominant feature and obscure signals from surrounding tissue. In nondestructive materials evaluation, the problem arises more frequently. In fact, structures are occasionally encountered which, by their very nature, are so highly reverberant that the reverberations comprise the entire received signal.

Jafar Saniie, born in Iran, received his B.S. in electrical engineering from the University of Maryland in 1974. In 1977 he received an M.S. in biomedical engineering from Case Western Reserve University and in 1981, a Ph.D. in electrical engineering from Purdue University. His research activities and interests include system identification and parameter estimation, digital signal processing, and ultrasonic imaging with both biomedical and industrial application. At present, he is in the Physics Department at the University of Helsinki, Finland, working on photoacoustics. Saniie is a member of Tau Beta Pi and Eta Kappa Nu.

Eric S. Furgason is an assistant professor in the School of Electrical Engineering at Purdue University. He did his graduate work on nonlinear acoustic interactions in dispersive structures and microwave acoustic signal processing, receiving his Ph.D. degree from Purdue University in 1974. Since joining the faculty, his research efforts have been primarily in the area of acoustic imaging and signal processing, for both medical and industrial applications, and acoustic flow measurement. He is a member of Sigma Pi Sigma, Tau Beta Pi, Eta Kappa Nu, ASNT, IEEE, and Sigma Xi.

Vernon L. Newhouse was born in Mannheim, Germany, and started his scientific career in 1944 working as a lab assistant for A. J. P. Martin who won the Nobel Prize in biochemistry. In 1952 he received the Ph.D. in physics from the University of Leeds, England, for studies on the ferromagnetic Barkhausen effect. For the next five years he worked on magnetic memory development and circuit design, first for Ferrauti in Manchester and later for RCA in Princeton and Camden, NJ. In 1957, he joined the G.E. Research Laboratory in Schenectady, NY, where he worked for 10 years on superconductive film computer devices. Since then he has worked at Purdue University, first on physical acoustics and later on ultrasound imaging and flow measurement. As of January 1982, he is the Disque professor of electrical engineering at Drexel University.

The particular problem of interest[1] arises in connection with in-service inspection of nuclear reactor steam generators. The objective was to develop a technique to measure, from inside a steam generator tube, the growth of support plate corrosion around the outside of the tube. Steam generators currently in use in certain nuclear reactors contain Inconel tubes which fit loosely in holes drilled through carbon steel support plates (Figure 1). Due to the high heat flux, there is a tendency for magnetite deposits to form on the inside surface of the support plate holes. When these deposits become too thick, they first touch and then dent the Inconel tubes, which can lead to their eventual fracture. If the magnetite formation were detected at an early stage, further growth could be prevented or reversed by chemical means.
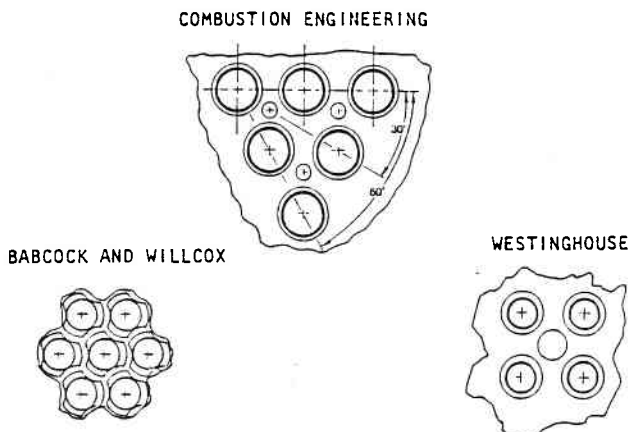

Figure 1—Cross-section of steam generator tube/support plate configuration (typical clearance 15 mils).

Ultrasonic imaging of these particular targets faces two major obstacles:
1. Severe reverberation in the tube wall causes echoes which overlap and mask the later occurring echoes from the tube/support plate crevice.
2. Tube wall thickness and the tube/support plate gaps were too small to measure accurately with transducers of readily obtainable bandwidth.

We begin the discussion with the formalism of the general problem and construct a simple model of the reverberation process. A wave classification scheme is introduced which permits the echo pattern of the reverberant structure to be systematically generated by computer simulation. The formal classification scheme and simulation are then applied to the particular problem of interest, steam generator tube/support plate structures, which consists of three layers.

Computer simulations of this particular structure lead to a second echo classification scheme which permits easy interpretation of the received signals. Experimental measurements on a planar model of the tube/support plate structure are used to verify the results of the simulations. The experimental results are then extended to the actual structure by development of a transducer assembly which fits within the steam generator tube. A simple signal processing technique is described and implemented which allows direct measurement of the tube/support plate gap to within approximately 1 mil.

REVERBERATION MODEL

For the sake of developing some insight and clarifying notation before analyzing the backscattered echoes from a highly reverberant discrete structure, we will first focus our attention on the simple case in which a thin film is examined by an ultrasound burst. The formalism thus developed can then be easily extended to analyze backscattered ultrasound echoes from a layered structure which is highly reverberant.

The problem of analyzing multiple reflections from a single thin layer has received some attention in the past.[2-5] In particular, Lees[3] used an analytical approach similar to the work by Redwood,[6] and developed a mathematical expression for reverberation echoes. Brekhovskikh[2] treated the steady state formulation of reflection and transmission coefficients from multiple layers in general, and a single layer in particular.

Previous work by Lees[4] and Rose[5] dealt principally with the reverberation echoes from a single isolated thin layer. Using conventional pulse-echo systems, these investigators studied the received reverberation echoes for the case where the duration of the incident sound pulse approximated or exceeded the travelling time in the thin layer. Under these conditions, it was reported that pattern recognition techniques are useful for film thickness measurement. In fact, the thickness of a film in the micrometer range can be measured with moderate accuracy from the ratio of the first pronounced peak to the next following peak of the echo signal.[3] Although pattern recognition techniques, such as the described peak-to-peak ratio test, are useful for thickness measurement of a single thin film, they cannot be easily extended to a structure composed of multiple layers in which each layer produces multiple echoes.

For a single layer system, the primary beam injected by the ultrasound transducer is partially reflected and partially transmitted at the front surface of the layer. The transmitted portion is subsequently reflected back and forth between the two surfaces of the layer. The received signal is therefore composed of multiple echoes which are detected at equal time intervals.

The mathematical expression for the successive received echoes is

$$(1) \qquad r(t) = \rho_{12} u(t) + \tau_{12} \tau_{21} \sum_{k=1}^{\infty} \rho^k_{23} \rho_{21}^{k-1} u(t - 2kT)$$

where ρ_{ij} and τ_{ij} are reflection and transmission coefficients of the adjacent ith and jth media respectively, and $u(t)$ is the impulse response of the system. The received echoes arrive at multiples of T which is the time it takes the echo to travel the thickness d of the layer. In principal, one would be able to measure the thin layer thickness very accurately by knowing the velocity, since the thickness is simply the product of the velocity and the time separation between received echoes.

The formula presented for a thin film can be extended to evaluate the characteristics of the received echoes from a multilayer media such as shown in Figure 2a. In the ultrasonic examination of this structure, the wave packet generated by the transducer enters boundary $B1$. At this point of discontinuity, part of the wave is reflected back toward the transducer while the rest is transmitted. The reflected echo is detected by the transducer at $B0$, while the original transmitted burst continues to travel toward boundaries $B2$ and $B3$. At $B3$ the wave is once again partially reflected and transmitted. The transmitted wave escapes into region $B\infty$ while the reflected echo passes through both $B2$ and $B1$, and is detected at a later time. Notice these echoes bounce back and forth and generate more wave packets at each of the discontinuities $B1$, $B2$, and $B3$.

In general, the echo will be detected after travelling n times in region II and m times in region III. Consequently, during a given scanning time t_0 the received signal is the summation of all these waves

$$(2) \qquad r(t) = \sum_{n=0}^{\infty} \sum_{m=0}^{\infty} \gamma_{nm} u(t - 2nT_2 - 2mT_3)$$

where γ_{nm} is the received echo amplitude related to ρ_{ij}, T_i is the travel time in the ith layer, and the condition

$$(3) \qquad nT_2 + mT_3 < t_0/2$$

must be satisfied for all n and m. In general, the term γ_{nm}

cannot be formulated in a closed form in terms of n and m. When $n=0$ and $m=0$, γ_{00} is the reflected echo from the boundary between region I and II, ρ_{12}.

An appropriate way to describe this reverberation phenomenon is by a closed network or equivalently by a tree structure, Figures 2b and 2c. In these figures, the nodes $B0$ and $B\infty$ are absorbing nodes representing the transducer and the unbounded support plate material. There is an amplitude and travel time associated with each node of the tree. However, from symmetry, many nodes represent equivalent values for both amplitude and travel time. After some given time many echoes which have travelled through these media following different paths can be detected. Discrimination of the individual travelling waves is quite complicated. To better understand the nature of the received echo, we have extended our work to wave classification using a computer simulation of the tree structure.
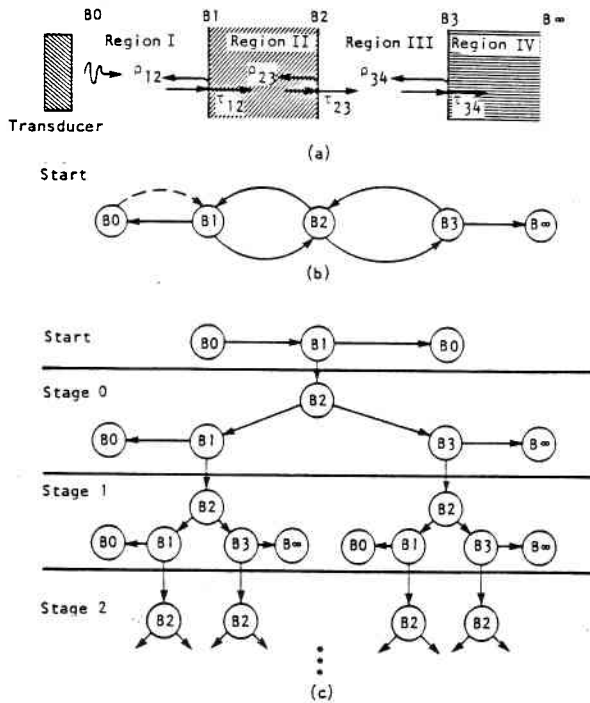

Figure 2—(a) Multilayer structure consisting of four layers; (b) equivalent network representation; and (c) tree structure of wave regeneration.

Classification Techniques

If the received echo signal from a layered structure is to be simulated during only a short time interval following the initial echo, a straightforward approach is simply to superimpose the signals corresponding to the various nodes of the tree (Figure 2c). However, if the time period to be simulated is somewhat longer, this approach rapidly becomes impractical because following the tree through only the first 20 stages leads to more than a million individual nodes. Fortunately, since many of these nodes represent wave packets with equivalent amplitudes and arrival times, a more efficient procedure is possible.

To simulate the backscattered echoes from the layered structure of Figure 2, the composite signal is decomposed into a series of unique echoes based on the following different characteristics. Type 0 echoes are those wave packets which traverse region II only once. Type 1 echoes are those wave packets which travel only once in region II and once in region III. Type 2 echoes are those wave packets which travel once in region II and twice in region III, and so on, as shown in Figure 3.

There exists a unique amplitude (A_i) and arrival time (t_i) corresponding to each type of travelling wave, as shown in Table I.

In general, a wave packet can travel by any path (Type 0 through Type N) or any combination of these paths. For example, the *type* of the pattern shown in Figure 4 is a combination of Types 1, 0, and 3. Based on this form of decomposition, any wave pattern can be represented in terms of our defined fundamental patterns. Following this scheme, there are many waves which travel via different paths but arrive at the same time and have the same amplitude.
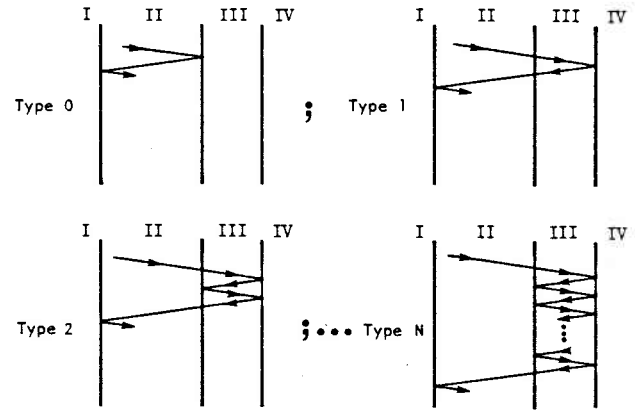

Figure 3—Elementary wave paths: Any wave path is a combination of the elementary paths.

TABLE 1

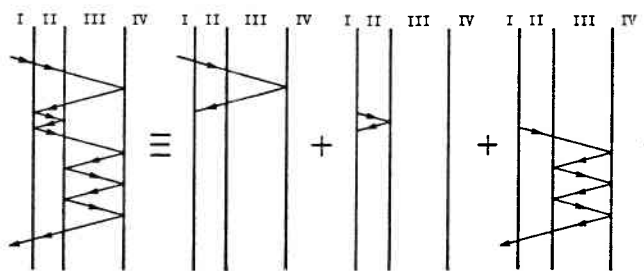| TYPE 0	$A_0 = \rho_{21}\rho_{23}$	$t_0 = 2\left[\dfrac{d_2}{C_2}\right]$
TYPE 1	$A_1 = \tau_{23}\tau_{32}\rho_{34}\rho_{21}$	$t_1 = 2\left[\dfrac{d_2}{C_2} + \dfrac{d_3}{C_3}\right]$
TYPE 2	$A_2 = \tau_{23}\tau_{32}\rho^2_{34}\rho_{32}\rho_{21}$	$t_2 = 2\left[\dfrac{d_2}{C_2} + \dfrac{2d_3}{C_3}\right]$
. . . . . .		
TYPE N	$A_N = \tau_{23}\tau_{32}\rho^N_{34}\rho^{N-1}_{32}\rho_{21}$	$t_N = 2\left[\dfrac{d_2}{C_2} + \dfrac{Nd_3}{C_3}\right]$

Figure 4—Decomposition of a given wave path in terms of elementary wave paths.

We can use the generalized binomial (multinomial) coefficients for estimating the number of equivalent paths,

(4)
$$N_{eq} = \frac{[\sum\limits_{i=0}^{N} K_i]!}{\prod\limits_{i=0}^{N} [K_i!]}$$

where K_i is the number of Type i wavelets. This method represents a more efficient technique for constructing the binary tree structure, shown in Figure 2, in the sense that it requires a minimal amount of computer computation and storage.

The amplitude corresponding to these equivalent waves can be calculated by using Table 1 and Equation 4,

$$(5) \qquad A_{eq} = \left(\frac{\tau_{12}\tau_{21}}{\rho_{21}} \right) N_{eq} \prod_{i=0}^{N} (A_i)^{K_i}$$

where the leading term represents the combined effect of the entrance into and exit from the first layer. These equivalent echoes are detected at times

$$(6) \qquad t_{eq} = \sum_{i=0}^{N} K_i t_i$$

Our computer simulations evolved another classification scheme based on the reverberations illustrated in Figure 5. An ultrasound burst entering region II from the left, will result in multiple reflections between the front and back surfaces which result in a class of echoes a_1, a_2, a_3, . . . which emerge from the left surface of the region at times $2(d_2/C_2)$, $4(d_2/C_2)$, $6(d_2/C_2)$, . . . where d_2 and c_2 are respectively the width and the velocity of the sound in region II.
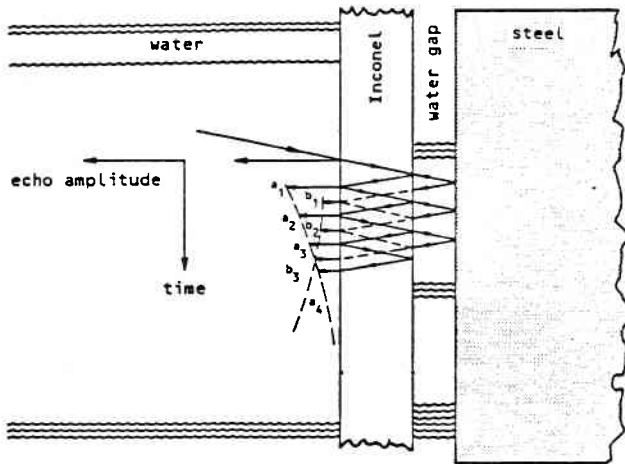

Figure 5—Tube/support plate cross-section showing multiple class 'a' and class 'b' echoes.

As indicated by the lengths of the arrows representing the class 'a' echoes, the height of echo pulse a_{n+1} is less than that of a_n due to energy loss at the boundaries of region II. Each time the incident sound reaches the back surface of region II, a small fraction of it passes into the water gap (region III) and reverberates between adjacent regions II and IV. Each time a sound packet returns to region II, a small fraction of its energy is transmitted through it toward the transducer. These rays are shown by broken lines in Figure 5 and emerge as a series of signals labeled b_1, b_2, b_3, . . . at times $2(d_2/C_2+d_3/C_3)$, $2(2d_2/C_2+d_3/C_3)$, $2(3d_2/C_2+d_3/C_3)$, . . . where the term d_3 is the length of region III and C_3 is the velocity of sound in region III.

Each time the 'a' type wave packet reaches the back surface of region II it generates a water gap wave packet which, upon returning to the region, adds energy to the 'b' series of signals. Thus the class 'a' pulses decrease with time whereas the 'b' series should actually increase with time, at least until it in turn loses energy to a 'c' type wave train (not shown in Figure 5). Class 'c' echoes consist of region II reverberations which have traversed region III twice. However, because such a ray passes from regions II and III four times, it loses most of its

energy. Therefore, the class 'c' echoes reaching the transducer will be negligible compared to the 'a' and 'b' class echoes, at least for the first few reverberations.

Based on the 'a', 'b', 'c', . . . classification, the generalized model for received echoes given in Equation 2 can be presented differently,

$$(7) \qquad r(t) = \rho_{12}u(t) + \sum_{k=1}^{\infty} a_k u(t-2kT_2) + \sum_{k=1}^{\infty} b_k u(t-2T_3-2kT_2)$$
$$+ \sum_{k=1}^{\infty} c_k u(t-4T_3-2kT_2) + \sum_{k=1}^{\infty} d_k u(t-6T_3-2kT_2) + \; . \; . \; .$$

where a_k, b_k, c_k, d_k, . . . are nonlinear functions of ρ_{ij}. The amplitude of class 'a' echoes can be expressed as

$$(8) \qquad a_k = \left[\frac{\tau_{12}\tau_{21}}{\rho_{21}} \right] A_0^{k-1}$$

According to the definition of class 'b' and using our wave-path decomposition the amplitudes of the 'b' echoes are

$$(9) \qquad b_k = k \left[\frac{\tau_{12}\tau_{21}}{\rho_{21}} \right] A_1 A_0^{k-1}$$

One of the major advantages of this wave classification scheme is that the class 'b' amplitude increases while class 'a' amplitude decreases. This increase is true for several reverberations, the exact numbers of which depend solely on the characteristics of region II (first thin layer). The effect of region IV (support plate) is to change the class 'b' echoes by an amplitude constant only.

In the specific case for which regions I and III are water (this is the situation in the tube/support structure) and using the relationship between τ_{ij} and ρ_{ij}, the b_n given in Equation 9 becomes

$$(10) \qquad b_n = n(1-\rho^2)^2 \rho^{2n-2} \rho_{34}$$

where $\rho_{12} = \rho_{32} = \rho$.

Evaluation of the above equation yields the conclusion that b_n is linearly related to the region IV characteristics (ρ_{34}). As the impedance of region IV increases, b_n increases which is a convenient situation for detection. Evaluation of b_n in terms of n and ρ is more involved. However, this can be accomplished by investigating the maximum of class 'b' echoes in terms of reverberation number n,

$$(11) \qquad \frac{\partial b_n}{\partial n} = \frac{\partial [n(1-\rho^2)^2 \rho^{2n-2} \rho_{34}]}{\partial n} = 0$$

Hence, the solution n for which b_n is maximum can be determined from

$$(12) \qquad n = -1/2\log\rho \qquad \text{for integer } n$$

The maximum value of b_n varies according to the characteristic impedance of region II relative to regions I and III. The reverberation is prolonged as the impedance of the thin layer increases. On the other hand, for a thin layer of lower impedance, the strongest 'b' echoes are the first few. A detailed evaluation of this effect is presented in Ref. 7.

To verify the above analysis of reverberations in the tube/support plate structure, a computer program was developed to simulate the output of a pulse-echo ultrasonic system operating in an A-scan mode. Figure 6 shows simulated A-scans of the tube/support plate structure for two different water gap widths. The upper trace of Figure 6 presents the case where the water gap delays the 'b' and 'c' echoes by an amount less than the reverberation time in the Inconel plate. In this plot, each class of echoes has a unique arrival time and the 'b' type echoes can be seen growing with respect to the type 'a' echoes. From this figure, the water gap size can be determined directly by measuring the time delay between the type 'a' and the type 'b' echoes.
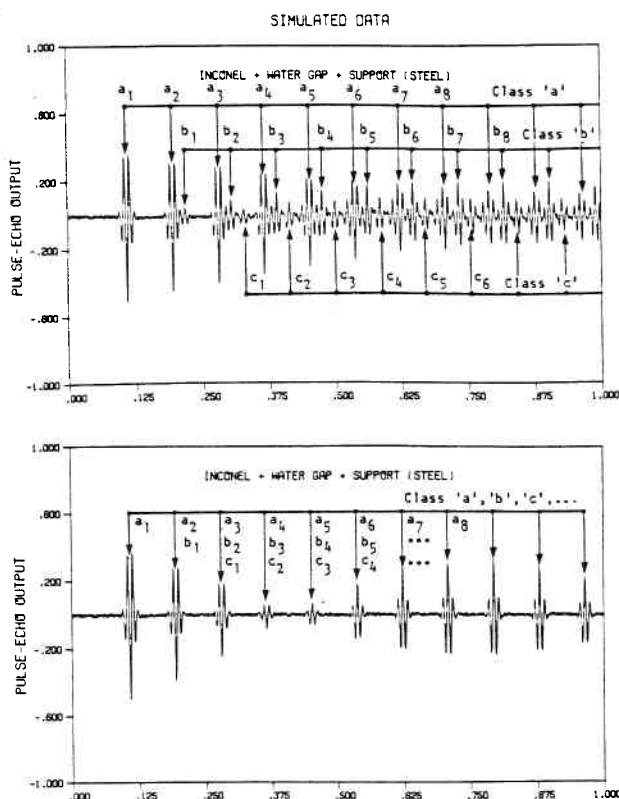
Figure 6—*Computer simulation of A-scans from the tube/support plate structure for two different water gap widths.*

Figure 7—Ultrasonic transducer assembly.

The transducer used in these experiments has approximately a 10 MHz bandwidth and a 20 MHz center frequency. The spatial resolution (ΔR) of the transducer is inversely proportional to transducer bandwidth, thus.

(13)
$$\Delta R \simeq C/2B$$

where C is the velocity of sound in the medium and B is the bandwidth. For this transducer, the resolution is 10 mils in Inconel which is smaller than the tube wall thickness, allowing the reverberation echoes from the tube wall to be readily resolved. The A-scan resulting from the pulse-echo operation of this transducer is digitized by sampling at 100 MHz with a Biomation 8100 transient recorder under microprocessor control and stored for additional signal processing. Figure 8 shows the overall system configuration.

Figure 8—Ultrasonic pulse-echo imaging system showing transducer orientation.

The lower trace of Figure 6 shows that a much different type of output is expected when the water gap delay equals the reverberation time within the Inconel tube wall. In this case, the 'b' type echoes cannot be uniquely identified although their presence is unmistakably shown by the rise of inverted echoes as time increases. As expected, for a whole range of water gap delays approximating the reverberation time in the Inconel, it is not possible to directly measure the water gap width from the A-scan. These plots clearly indicate that it is possible to measure the water gap width, although additional signal processing of the A-scan may be necessary when the class 'a' and class 'b' echoes are not resolvable.

DATA ACQUISITION

Experimental measurements were obtained by the transducer assembly shown in Figure 7. In order to avoid near field characteristics and multiple reflections between the transducer and the tube wall, a delay path was introduced by using an acoustical mirror. The mirror was mounted at a 45 degree angle with respect to the transducer causing the deflected sound wave to be perpendicular to the tube wall. During reception, reverberation echoes from the tube wall and support plate propagate back to the mirror and are projected onto the transducer element.

The experimental transducer element and mirror are rigidly mounted in a housing which centers the transducer in the Inconel tube. The transducer housing has sliding seals which allow the assembly to be pushed along the tube or rotated on its axis but which still securely holds the transducer in place during measurements. The transducer head is attached to a wand which permits rapid insertion, easy movement, and accurate positioning of the probe by hand for laboratory measurements.
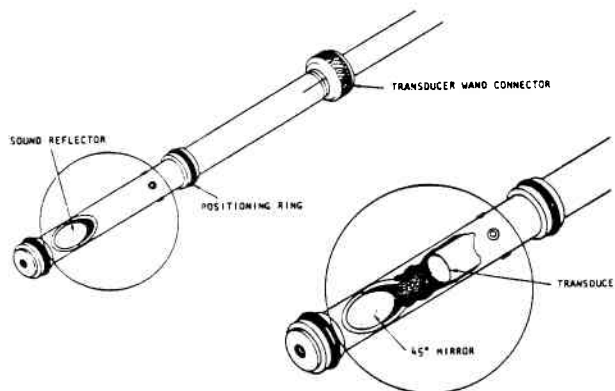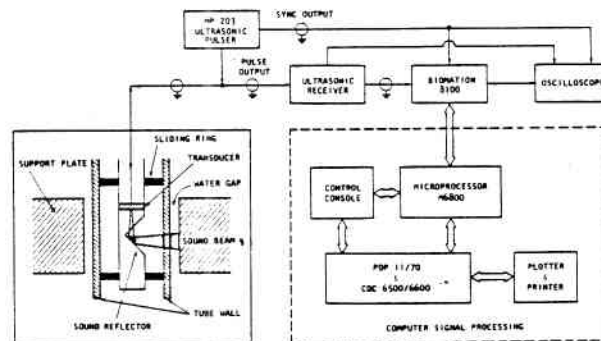
The digitized data has poor signal-to-noise ratio which is basically due to the uncertainty in the timing of the sampling interval, especially when operating at 100 MHz. Since the statistical properties of the entire sampling process are unknown, the reduction and compensation of the noise signal by filtering would be quite difficult. However, by incorporating coherent averaging, the signal-to-noise ratio of the measured signal was improved significantly.

Further signal processing involved decomposition of class 'a', 'b', . . . echoes. Direct decomposition can be achieved by a simple subtraction scheme. In addition to the echo signal from the tube/support plate gap, the subtraction technique also requires the collection of a reference signal from the steam generator tube in a region away from the support plate assembly. Generally the tube and tube/support signals have the same arrival time (i.e. synchronized) which allows direct subtraction. The subtraction technique works well only when the signal-to-

noise ratio is high and the reference signal is closely matched to class 'a' echoes.

EXPERIMENTAL RESULTS

To test the foregoing classification scheme and computer simulation, we set up a test structure consisting of a flat 56 mil thick Inconel 600 plate, separated by a water gap from a much thicker carbon steel plate. This structure exactly simulates the Inconel tube-support geometry of steam generator tubing (Figure 1) except for the fact that the simulation structure is flat whereas the Inconel tube-support plate is cylindrical. The reverberation pattern of this structure, when irradiated with a transducer of 20 MHz center frequency and 10 MHz bandwidth, is shown in Figure 9.

The upper A-scan in Figure 9 shows the reverberation echoes produced by just the 56 mil Inconel flat in a water bath. As expected, the uniformly spaced class 'a' echoes decrease with time as energy leaks from the reverberating wave packet into the surrounding water bath. The center trace shows the effect of positioning a flat carbon steel plate behind the Inconel flat in such a way as to leave a water gap of approximately 10 mils. In this trace, the beginning of the signal is dominated by class 'a' echoes. However, as the time advances, the class 'b' echoes emerge after the class 'a' echoes. This process becomes accentuated around the 8th 'b' echo as predicted by Equation 12.

Although the addition of the support plate introduces both class 'b' and 'c' type echoes, their exact location is not easily resolved. By subtracting the reference signal (upper trace), the class 'a' signals can be removed, clearly revealing the location of the class 'b' and 'c' echoes. The bottom trace of Figure 9 shows the result of this simple processing. In this trace, the inverted 'b' type echoes are easily identified and show the characteristic increase in amplitude with increasing time. Finally, the water gap width is determined from the measured delay between type 'a' echo and its associated type 'b' echo as shown in the figure.
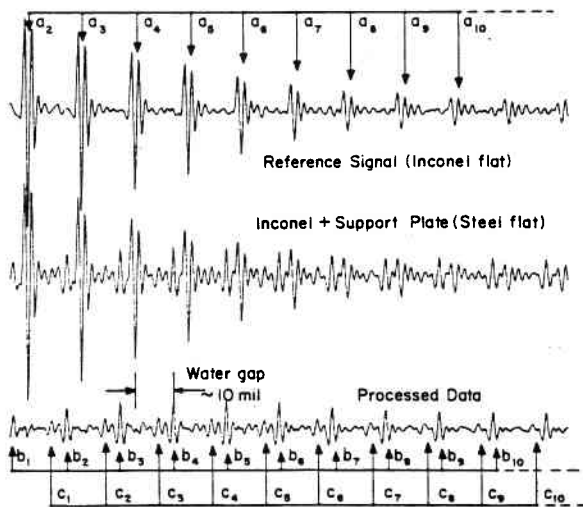

Figure 9—Experimental measurement of the water gap in planar model of tube/support plate structure.

The potential of this technique for monitoring the growth of magnetite in tube support plate holes is established by the following measurements. The first series of tests, performed on a length of steam generator tube mounted in a section of carbon steel support plate, is presented in Figure 10. The uppermost trace in this figure was obtained by positioning the transducer assembly within the tube, in a region away from the support plate. After obtaining the reference signal, the Inconel tube and transducer assembly were both slid through
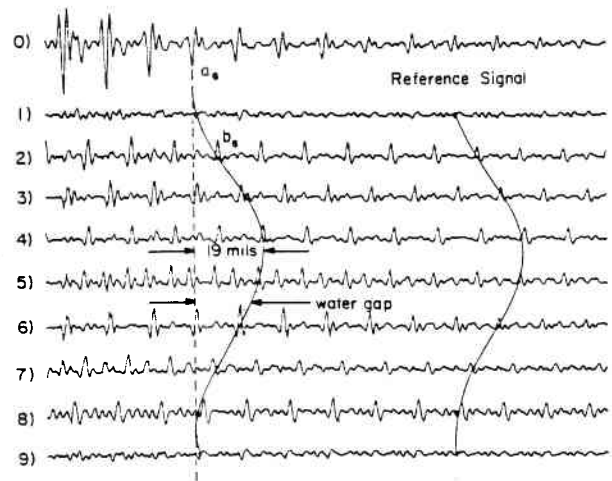

Figure 10—Experimental measurement of water gap in tube/support plate structure: Inconel tube 750 mil O.D., support plate hole 765 mils.

the support plate hole until the transmitted ultrasound illuminated the center of the support plate hole. In these tests, the transducer assembly remained stationary within the steam generator tube to prevent changes in the transducer orientation which might alter the reference signal.

The first trace of processed data (second trace from the top) represents the case of near contact between the support plate and the tube. The water gap width in this case can be determined from the time separation between the nth type 'a' echo of the reference signal (top trace) and the corresponding class 'b' echo of the processed signal (second trace). Each of the following traces were produced as the off axis position of the tube was changed in the direction of increasing water gap width. This series of experimental plots shows that changes in the water gap width can easily be monitored with this technique with an accuracy of better than 1 mil, at least for this idealized case.

The second set of experimental results, Figure 11, displays the performance of the prototype system under more realistic conditions. In this case, the Inconel tube was securely held in place, offset in the hole, so that at one point the outside of the steam generator tube was in contact with the support plate. This arrangement represents the worst case, in terms of tube orientation, for this type of water gap measurement.

The uppermost trace in Figure 11 is again a reference signal obtained away from the support plate intersection. After this reference signal was obtained, the transducer assembly was slid along the inside of the Inconel tube to the support plate intersection and then rotated. Each of the traces, 1 through 8, represents processed output from the prototype system obtained by rotating the transducer assembly by hand through approximately 45 degrees of arc. Thus, trace 1 is from a point very near the point of contact between the tube and support plate, and trace 9 was produced after a rotation of 360 degrees or one complete revolution and corresponds to approximately the same location as trace 1. The broken vertical line in this figure is drawn from the negative peak of the reference signal, which is known to correspond to the outer surface of the steam generator tube. If the distance between this plane and the corresponding class 'b' echo is measured, the water gap width can be determined directly.

The accuracy of our measurement technique is demonstrated by the solid curve (nearest the broken line) which represents the calculated water gap distance based on actual measurement of the physical dimensions of the support plate hole and tube diameter. The agreement between the direct measurements and the ultrasonic gap measurement is shown to be consistently